PORE WATER INFILTRATION AND DRAINAGE ON A MEGATIDAL BEACH IN RELATION TO TIDE- AND WAVE-FORCING

Nina Stark[1], Alex E. Hay[2]

A pressure and temperature sensor (pT sensor) was deployed at mid-tide level and at a sediment depth of 0.5 m on a steep, megatidal, mixed-sand-gravel beach in Advocate Beach, Bay of Fundy, Nova Scotia, for pore pressure monitoring at the beachface. The pT sensor was buried at a sediment depth of 0.5 m centrally located in the intertidal zone. For comparison, another pT sensor of the same model was synchronized and mounted to an instrumented frame 0.5 m above the beachface at approximately the same location. The tidal range in this area is ~ 10-12 m. During the experiment, significant wave heights ranging from 0.1-0.9 m and wave periods ranging from 3-8 s were measured. The results demonstrated that the pT sensor was well suited for pore pressure monitoring with regard to tidal variations and wave action in the intertidal zone. A spontaneous infiltration of pore space with the uprising flood tide was observed, while the drainage phase was extended in response to low drainage rates. Regarding wave action, the wave signal was well reflected in the pore pressure records. However, the signal was damped and delayed compared to the in-water pressure signal. Also, wave skewness and asymmetry was more pronounced in the sediment. Despite the very coarse material (d_{50}=0.3-18.5 mm), short phases of pore pressure build up were observed. Based on this data set, a more detailed analysis of pore pressure signals with regard to surficial grain size variations and hydrodynamics will be carried out.

Keywords: pore pressure; gravel-sand beach; swash; surf

INTRODUCTION

Variations of pore pressure and liquefaction in beach and coastal sediments play an important role for sediment stability and sediment dynamics in the coastal zone. Recently, these issues have come to the fore with an increasing awareness of their impacts on coastal erosion, offshore and coastal structures. Sediment liquefaction is often associated with earthquakes. However, scientists and engineers recognized the risk of liquefaction of marine sediments due to storm events and wave action at least as far back as the 1970s. Bjerrum (1973) pointed out that offshore structures in the North Sea are potentially at risk due to liquefaction of sands during storm events, while Dalrymple (1979) connected slump-like morphological deformations in the Bay of Fundy to possible liquefaction due to wave action. The latter also hypothesized the possibly stronger impact of breaking waves, compared to passing wave trains. Sakai et al. (1992) reported sinking concrete blocks at a beach in Japan, and proved that liquefaction is a theoretically consistent explanation for the observed beach sediment instability. Such theories were supported by laboratory studies by, e.g., Clukey et al. (1985); Sassa and Sekiguchi (1999).

Two processes of liquefaction have been discussed in coastal research: i) residual liquefaction, being based on pore pressure build up and well known from earthquake engineering; and ii) momentary liquefaction or fluidization, following major pressure variations and flow in the pores of the surface sediment layers (Mutlu Sumer, 2014). In subaquaeous environments, the former relates to pore pressure build-up in response to the hydrostatic pressure fluctuations of passing wave trains (Fig. 1), as well as vibration of structures or seismic activity. Since the 1990s researchers have successfully demonstrated and investigated this effect in wave tanks and numerical simulations (Sakai et al., 1992; De Wit and Kranenburg, 1997; Sassa and Sekiguchi, 1999; Osinov, 2000; Sassa and Sekiguchi, 2001; Jeng et al., 2004; Mutlu Sumer et al., 2006). Momentary liquefaction has gained in importance regarding observations of unexpectedly strong erosion, for example at beaches during storm events and in connection with scour. It corresponds to a break up of the sediment matrix due to a strong flow in the pore space of the upper sediment layers. In the nearshore zone this mainly results from energetic wave action which lead to strong flows at the seabed, as well as to breaking waves impacting the seabed and swash (Fig. 1) (Mutlu Sumer, 2014).

Physical simulations were conducted in which liquefaction due to wave action was successfully demonstrated (Nataraja and Gill, 1983; Sassa and Sekiguchi, 1999; Mutlu Sumer et al., 2006). Numerical models were developed to investigate this issue in more detail and for more specific scenarios (Jeng, 1996; Sassa and Sekiguchi, 2001). However, there is a lack of field data. Field observations of structure instability and strong morphological changes have served mainly as motivation for follow-on detailed investigations of the sediments and scenarios in the laboratory and numerical simulations, but actual pressure monitoring

[1]Department of Civil and Environmental Engineering, Virginia Tech, U.S.A.
[2]Department of Oceanography, Dalhousie University, Canada

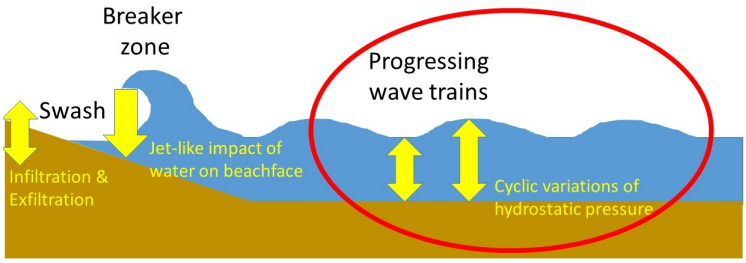

Figure 1: Conceptual sketch of wave characteristics which influence pore pressures in beach sediments. The here presented results focus on progressing wave trains (red circle) and tides.

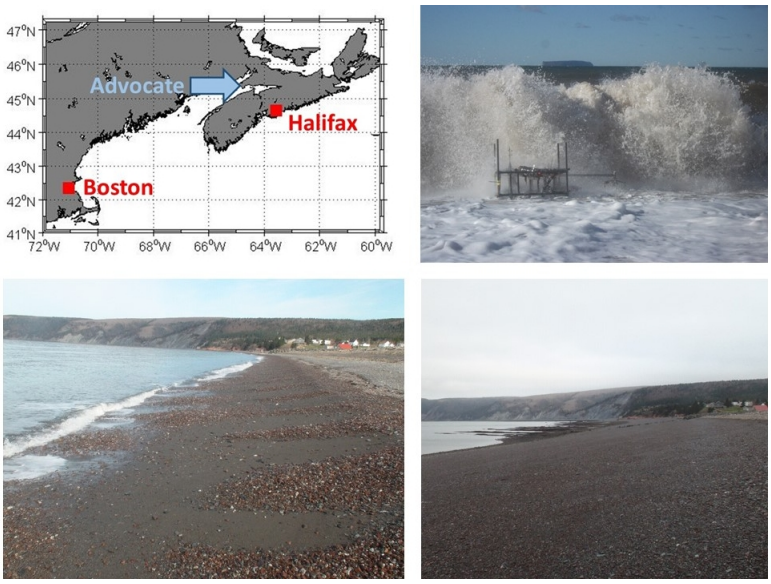

Figure 2: Upper left) Map of the Gulf of Maine and the Bay of Fundy indicating Advocate Beach (blue arrow). Upper right) Shorebreaks during a storm event. The upper horizontal bars of the instrumented frame has a height of ~ 0.5 m. Lower panels) Images from Advocate Beach.

under wave action has rarely been conducted. Buried pressure sensors have been deployed with focus on swash and infiltration/exfiltration of beach sediments and have provided insight into possible momentary liquefaction in the swash zone (Turner and Masselink, 1998; Butt et al., 2001; Nielsen et al., 2001; Turner et al., 2008). However, a number of research questions have yet to be addressed: How do variations in grain size, sorting and grain shape impact the risk of liquefaction? At which sediment depths does pore pressure build up occur depending on wave characteristics? What are the effects of nearby stiff or possibly vibrating coastal structures?

To address those questions, pore pressure monitoring at different sediment depths over several tidal cycles, different wave conditions and active sediment transport are required, and the understanding of pore pressure response to different hydrostatic conditions has to be improved. In this article, we present preliminary results from pore pressure measurements at a highly active mixed-sand-gravel beach in Advocate, Nova Scotia, covering 23 tidal cycles.

REGIONAL CONTEXT

Advocate Beach is located in Nova Scotia, Canada, facing the open Bay of Fundy and Gulf of Maine (Fig. 2). It is characterized by a large tidal range of ~12 m and a steep beach slope of ~7°. Grain size distributions are highly variable in time and space and range from sands (particle diameter d ≤2 mm) to cobbles (d ~150 mm and larger). The sandy fractions stand out due to their elliptic-plate-like shape and

high friction angles ($\phi \approx 40°$) (Stark et al., 2014). Significant sediment transport of the finer fractions can mostly be associated with the formation and destruction of ripples by the swash and surf zone, forming an up to ~10 cm thick beach cover of sandy sediments during storm conditions (Hay et al., 2014).

Two pilot experiments were carried out at Advocate Beach in May 2012 and in October–November 2013 with the aim to test novel measurement devices and survey strategies spanning both low and high energy wave conditions. During the May 2012 experiment, median grain sizes varied temporally and spatially between d_{50}=0.3-18.5 mm, showing a cross-shore zonation with four distinct zones from the low tide level to the berm (Stark et al., in prep.), the formation of sorted beach cusps at the low and high tide level (Fig. 2) and fine sediment beachface coverage following the formation and destruction of ripples during a storm event (Hay et al., 2014). At a sediment depth of ≥20 cm, the median grain size remained approximately constant at 3.5-4 mm (Stark et al., in prep.). Significant wave heights reached $H_{1/3} \approx 0.9$ m during the May 2012 experiment.

METHODS

Two pressure and temperature sensors (pT sensors) of the model *RBR Duo TWR-2050* were deployed from April 30^{th} to May 15^{th} 2012. One was mounted to an instrumented frame (Fig. 2) at a height of ~0.5 m above the beachface, while the other one was attached to a ~7.5 kg lead weight and buried at a sediment depth of ~0.5 m in the immediate vicinity of the instrumented frame. The frame was located approximately in the center of the intertidal zone with regard to the cross-shore direction. The pT sensors sampled continuously at 4 Hz. Tidal variations were recorded as 5 minute averages. Wave data was collected in bursts every thirty minutes for fifteen minutes.

RESULTS

Both sensors withstood the harsh conditions at Advocate Beach. Despite heavy wave action during a storm event and burial, both sensors worked well without any damage or data loss. Batteries as well as memory were still available after the measurement period of 16 days.

The pore pressure signals of the buried as well as frame-mounted pT sensor reflected the lunar and semidiurnal tidal variations. The pressure profiles of the two differently located pT sensors matched well as soon as the water depth exceeded 0.5 m, when the frame-mounted pT sensor was fully submerged (Fig. 3A). This is revealed particularly well by plotting the time derivative of the pressure (dp/dt; Fig. 3B). Focusing on the infiltration of pore space, a peak in dp/dt ≈0.03-0.05 dBar/minute is reached within one averaging interval (5 minutes), indicating rapid infiltration (Fig. 3). After this peak, dp/dt decreases approximately linearly until the frame-mounted pT sensor is exposed to air again. As expected for this sensor, the frame-mounted sensor represented the tidal cycle without any deviations. The buried pressure sensor on the other hand, showed a signficantly different pressure progress during the retreating ebb tide. Approximately at 0.4 dBar above atmospheric pressure, the rate of pressure decrease slowed down signficantly, and a drainage rate of only -0.005 dBar/minute was maintained over ~1-1.5 hours until the pressure returned to atmospheric pressure. The described behavior, including similar infiltration peaks, drainage rates and drainage times, were observed during all measured tidal cycles.

Analysis of the non-averaged burst data recorded at 4 Hz showed that differences in wave action were clearly reflected in the data of the buried pT sensor. At a sediment depth of 0.5 m, energetic wave action during a storm event as well as very limited pressure fluctuations were still noticeable (Fig. 4). During the storm event, short phases of pore pressure build up were identified (Fig. 4 upper panel from 2-18 s). Looking at the wave-resolving data on a larger temporal scale, the results reflected the wave activity over different tidal cycles and during the different phases of the tidal cycle (Fig. 5). Significant wave heights H_s (Thornton and Guza, 1983) increased significantly during a storm event between yearday 129–133 (Fig. 5 lower panel), and the largest significant wave heights over single tidal cycles during this storm event were registered by the buried pT sensor for the passing surf on the rising tide (Fig. 5).

The wave-resolving data was analyzed in more detail by comparing the buried to the unburied pT sensor. Figure 6 shows a representative pressure elevation time series at different scales. The specific wave characteristics shown by the unburied pT sensor were clearly identified in the buried sensor's time record. However, the following differences were noted: First, the wave signal registered by the buried sensor appeared damped in amplitude. Second, pore pressure relief was delayed and was sometimes not achieved at all, meaning the pore water pressures were sustained over the passing wave trough. Third,

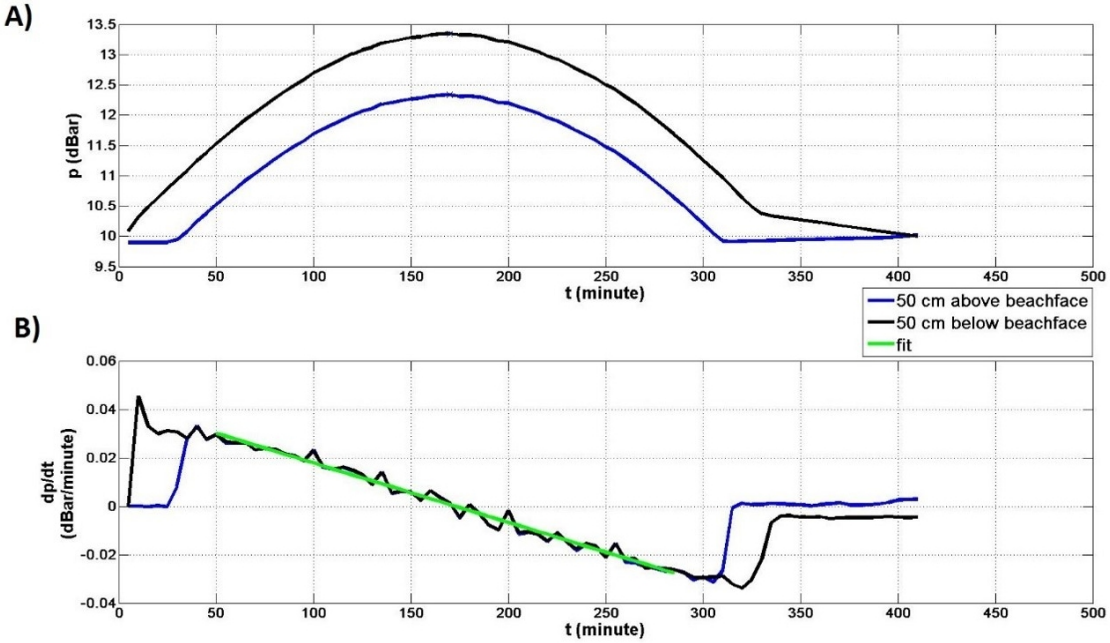

Figure 3: Exemplary data set of one tidal cycle. The frame mounted pT sensor is represented by the blue line, while the buried pT sensor is shown in black. A) Time versus pressure; B) the change of pressure over time versus time. The green line represents a linear fit.

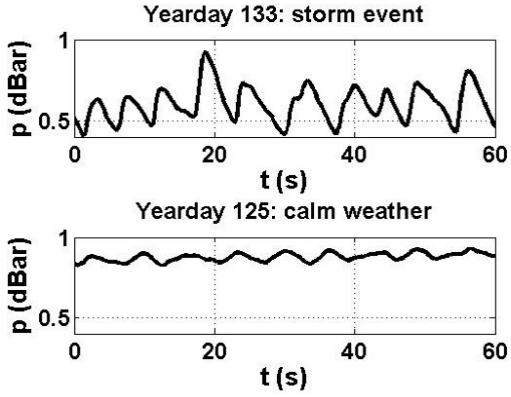

Figure 4: Two representative minute-long records of pressure fluctuations with regard to wave action. Both data sets were recorded at 6 Hz and are not time-averaged. Atmospheric pressure has been removed.

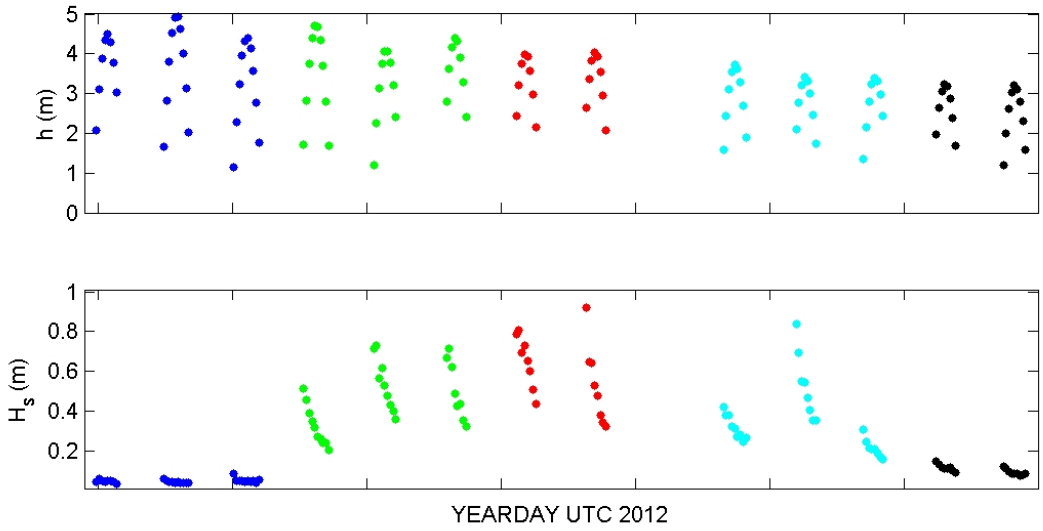

Figure 5: Water depth h measured at a sediment depth of 0.5 m below beach surface (upper panel) and significant wave height H_s (Thornton and Guza, 1983) (lower panel) over thirteen tidal cycles including pre-storm (blue), early- (green), mid- (red), late- (light blue) and post-storm event (black).

the signal at the buried sensor was observed to lag the unburied one. The described differences in wave characteristics were also investigated in terms of of skewness and asymmetry. We note that the pressure signal from the unburied sensor was not corrected for Bernoulli effects since – as the significant wave orbital velocities were less than 1 m/s (Hay et al., 2014) – the corresponding elevation signal would have been less than 5 cm. Figure 7 shows the correlation of skewness and asymmetry in the wind wave band. The results confirmed that the wave characteristics at a sediment depth of 50 cm differed from the characteristics of the same wave at 50 cm above the beachface. Wave skewness was more pronounced at the buried pT sensor i.e. more positive. Negative asymmetry was also larger at the buried sensor, expressing a steeper wave front facing the shore (Fig. 7). (Note, the asymmetry values in figure 7 are for the time domain: i.e. negative values indicate wave fronts leaning backward in time.)

The damping effect was also reflected when comparing the wave energy spectra of the buried pT sensor to the unburied pT sensor (Fig. 8 left). The respective spectral ratio remained approximately constant across the surface gravity wave band over the respective single tides (Fig. 8 right). The spectral ratio was also examined depending on different stages of a storm event that hit the beach during the experiment (Fig. 5 and 9). With regard to wave frequency within the surface gravity wave band (Fig. 9 left), the spectral ratios were significantly lower ($\sim$ 0.3-0.8) for the late- and post-storm data sets compared to the pre-, early- and mid-storm data ($\sim$ 0.6-1). When plotting the spectral ratio versus water depth (Fig. 9 right), the spectral ratio increased approximately linearly from about 0.3-0.6 at a water depth of $\sim$ 1 m (both sensors just submerged) to 0.8-1 when reaching a water depth of 4 m at high tide.

The squared coherency and phase between the buried and the unburied pT sensor data sets was examined. Coherency in the incident gravity wave band was well within the 95% confidence level (Fig. 10). The wave spectra were characterized by a low-frequency phase ramp, as well as allowed to determine a mean phase in the wave band (Fig. 10). More detailed data analysis is still ongoing. However, preliminary results suggested that neither phase ramp nor mean phase over the wave band were dependent on energy-weighted mean frequency, while the phase ramp showed an increase of phase with decreasing water depth.

DISCUSSION

The pT sensors which were originally designed as tide and wave gauges proved useful for pore pressure monitoring in the beachface over a measurement period of 15 days. The battery and memory left suggested that the instruments could easily record at the applied configurations for a month or longer. The sensors also performed well in harsh shorebreaks and buried in the sand-gravel mixture. As far as we have been able

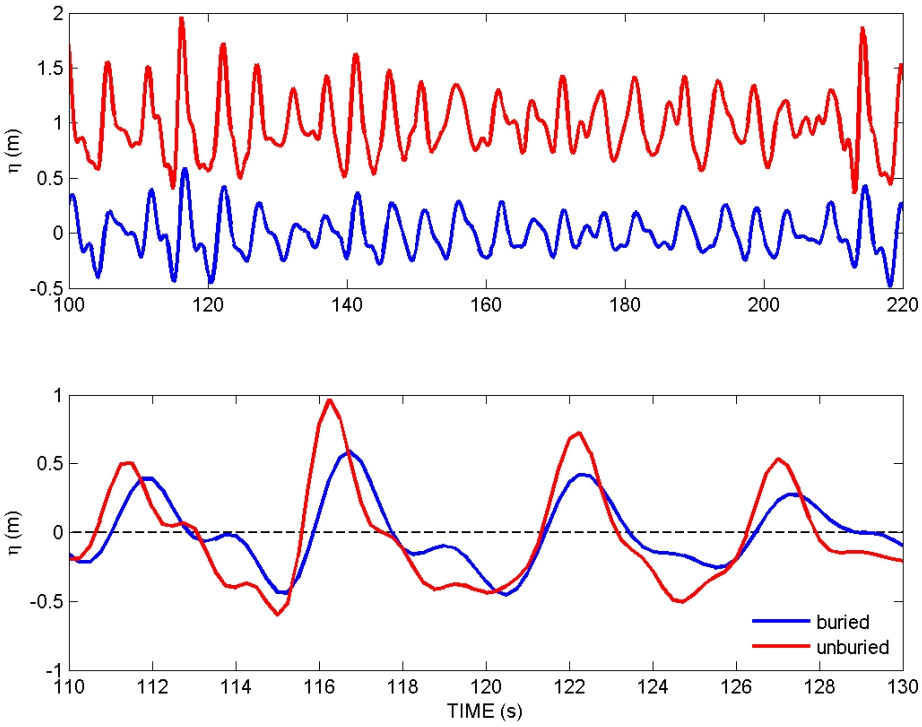

Figure 6: Pressure elevation time series showing a 2-minutes segment (upper panel) and a 20 s segment (lower panel) from the time characterized by the largest significant wave height on yearday 133 (Fig. 5 upper panel). The unburied pT sensor (red) was located 1 m above the buried sensor (blue). This offset in height was removed in the zoomed-in data set (lower panel). Particularly, the zoom shows a time lag and the incomplete and/or delayed pore water pressure relief.

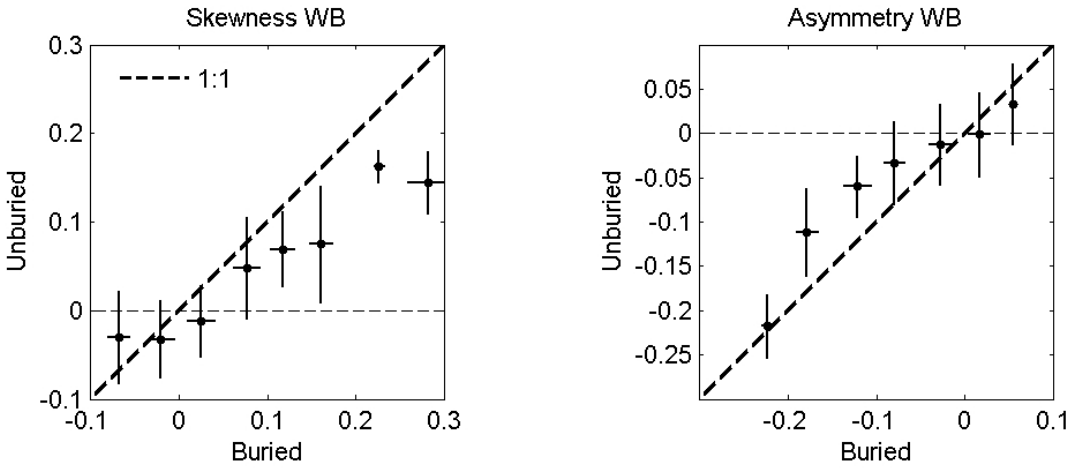

Figure 7: Skewness (left) and asymmetry (right) of the buried pT sensor versus the unburied pT sensor in the wind wave band 0.1-0.33 Hz.

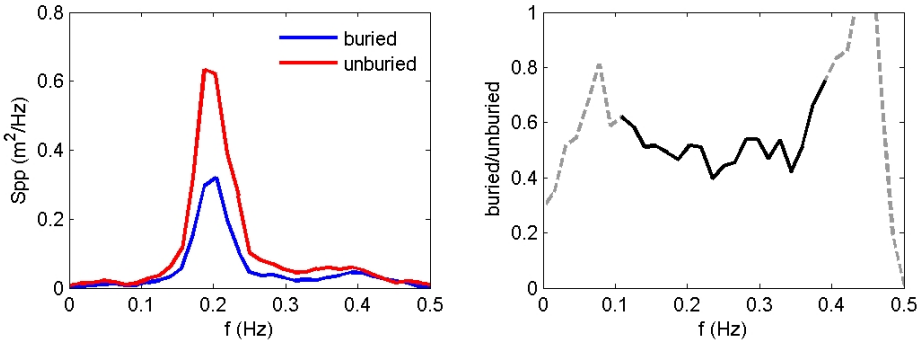

Figure 8: Wave energy spectra derived from the buried (blue) and the unburied (red) pT sensors (left), and the buried/unburied spectral ratio (right). In the latter, the black line indicates the 0.1-0.33 Hz frequency range over which the incident gravity wave band was computed. These spectra were computed for the full 17-min run from which the data segments in figure 6 were taken.

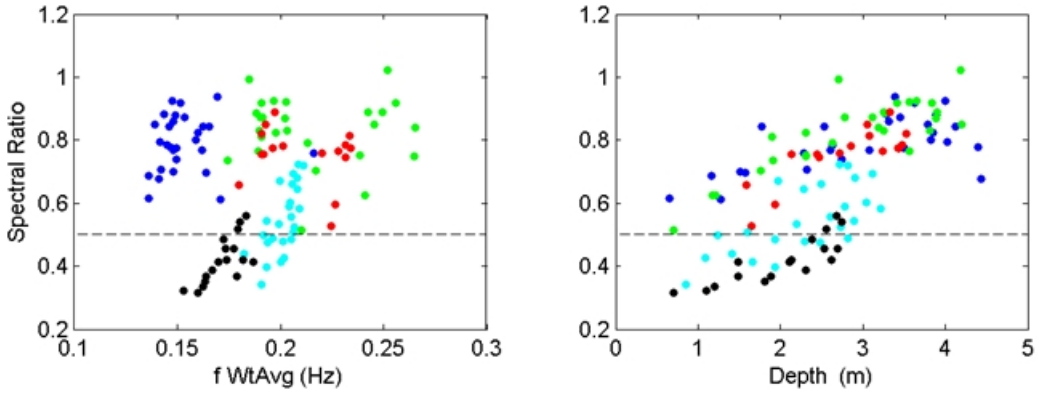

Figure 9: Wave band spectral ratios (Fig. 8) spanning the storm event (color coded as in figure 5) vs. energy-weighted mean frequency (left) and water depth (right).

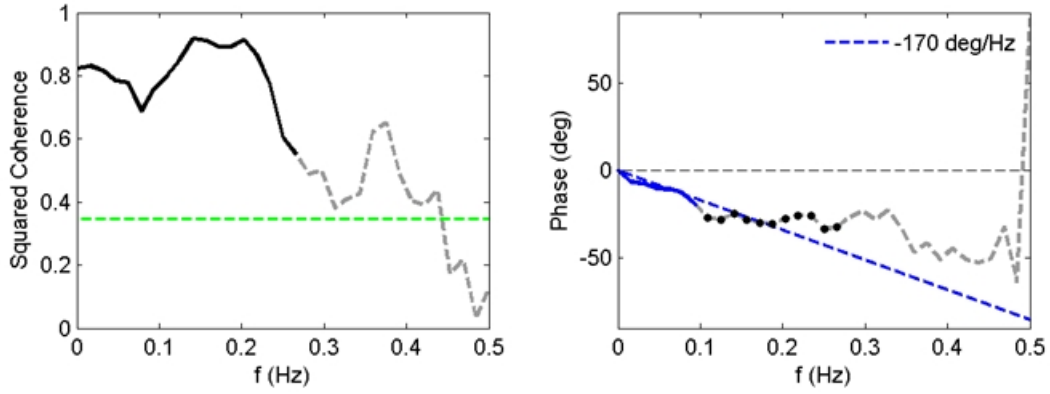

Figure 10: Left) Squared coherence spectrum. The dashed green line indicates the 95% confidence level, while the solid black line indicates values >0.5. Right) Phase spectrum. From the phase spectra a low frequency ramp was determined (blue dashed line) based on the low frequency data highlighted in blue, as well as the mean phase in the wave band satisfying a squared coherence >0.5 criterion indicated in black. These spectra were computed from the same data as those in figure 8.

to determine to date, concerns about sensor clogging by sediment were not realized. However, this might become an issue with finer sediments, and a screen protecting the water inlet might be required. Generally, the pT sensors performed very well, and allowed an easier set up with potential for deployment and deeper water environments than a cabled configuration (Turner and Masselink, 1998).

A rapid infiltration of the pore space in the sediment matrix was observed (Fig. 3). If pores are flushed rapidly with water, this can affect the strength of the sediment matrix, and might lead to an easier sediment mobilization during this phase (Horn, 2002). As most of the sediment remobilization at Advocate Beach was observed in the swash and following surf zone (Hay et al., 2014), this factor might have indeed had a significant impact. The drainage phase was characterized by a slow drainage rate and an extended drainage phase of over an hour (Fig. 3). To our knowledge, this has not been previously documented to this extent, and might have a significant impact on sediment mobilization during the passing swash and surf zone of the retreating ebb tide. However, in a more detailed investigation, the temperature signatures will be utilized to identify air ventilation of pores and the impact of groundwater dynamics to shed more light on this issue.

Wave characteristics were still reflected in sediment depths of 0.5 m, highlighting that pore water fluctuations down to a significant depth are influenced by rapid hydrostatic fluctuations (Fig. 4) increasing the risk for liquefaction, particularly at shallower sediment depths (Mutlu Sumer, 2014). However, damping and distortion of the original hydrostatic wave signal were indicated. Specifically, the wave signals in the sediment were damped in amplitude, showed a delayed and sometimes an incomplete pore water pressure relief during passing of the wave trough, and lagged in time (Fig. 6 and 8). Damping, expressed through a low spectral ratio, was particularly pronounced during the late and post-storm event phase, as well as at low water levels (Fig. 9), but was largely independent of energy-weighted mean wave frequency (Fig. 9) and also significant wave height (not shown). Based on the currently analyzed data, it seems likely that this may result from active sediment dynamics depending on the wave forcing, leading to variations in surficial grain size distribution and bed roughness in the upper 20 cm of the beachface. Hay et al. (2014) described the formation and destruction of ripples at the beach surface by the passing swash and surf zone during flood and ebb tide, respectively. This resulted in significant variations of surficial grain size distributions during the late and post-storm event period (Hay et al., 2014; Stark et al., in prep.). In addition to ripple formation and destruction, the response to water depth may result from the respective location of the surf zone and the following changes in wave characteristics, as well as possibly the impact of groundwater dynamics. With regard to the latter, differences between flood and ebb tide would be intuitive, however, such differences were not identified.

Wave skewness was larger (more positive) at a sediment depth of 0.5 m, as well as asymmetry (more negative). These observations likely resulted from the delay in pore water pressure relief and sustaining of pore water pressure, and suggested that even in such coarse sediments (sandy gravel) wave and hydrostatic pressure characteristics are deviated and that the assumption that pore water pressures mirror hydrostatic conditions cannot necessarily be supported.

Short phases of pore pressure build up were observed which followed the idea of a steady increase as documented by e.g. Mutlu Sumer et al. (2006). This behavior based on above described observations of sustained pore pressures over single and small groups of waves. However, the elevated pore pressure was relieved before sediment effective stresses were reached and liquefaction could occur. This is in accord with expectations following the coarseness of the sediment mixture. Nevertheless, the fact that pore pressure build up was observed at all and that such build up phases were observed in correspondence to passing wave trains suggested that under energetic shorebreaks and in shallower sediment depths momentary as well as residual liquefaction cannot be excluded as a factor amplifying erosion. More investigations are required to address this issue. In a follow-up experiment pT sensors were deployed at sediment depths ranging from 10-50 cm at different locations along the beach's cross-shore profile.

CONCLUSION

The following conclusions can be drawn from a preliminary data set of a buried pressure-temperature sensor, deployed at a mixed sand-gravel beach for a period of 15 days:

1. Pressure-temperature sensors which were designed as tide and wave gauges performed well for pore pressure monitoring at a mixed sand-gravel beach over a measuring period of 15 days.

2. Spontaneous infiltration with approach of the flood tide, and delayed and slow drainage of pores

during retreat of the ebb tide was observed.

3. At a sediment depth of 0.5 m, damping of wave-dependent hydrostatic pressure variations, time lags and sustaining of pore pressures were monitored. This led to a change in wave characteristics when comparing the same wave signal with a buried versus an unburied pT sensor.

4. Short phases of pore pressure build-up were identified.

This study represented a first attempt to utilize pT sensors which have been designed as tide and wave gauges for pore pressure monitoring in beach sediments. The sensors proved to be useful, and preliminary data analysis was presented. However, the results also stressed the need for more detailed investigations. Different trends with regard to deviations of the wave characteristics at a sediment depth of 0.5 m from the hydrostatic signatures were identified, but more data and analysis is required to develop and support hypotheses explaining the observations. Next steps will include a detailed analysis and correlation of temperature variations to the pressure fluctuations and hydrodynamics, as well as a correlation of the changes in wave characteristics to surficial grain size and water level. A follow-up experiment was conducted at the same location deploying a full cross-shore array of pT sensors at a sediment depth of 15 cm and a vertical array with three pT sensors at a sediment depth of 10, 25 and 50 cm centrally at the beachface. This data set is currently being processed, and is expected to give further insights.

ACKNOWLEDGEMENTS

The Advocate 2012 field experiment was funded by the Natural Sciences and Engineering Research Council of Canada, the Atlantic Innovation Fund and Nortek. We thank the Advocate Harbour experiment field team: R. Cheel, D. Barclay, M.G. Hatcher, J. Hare, T. Guest, D. Schillinger, G. Wilson, L. Zedel and W. Judge. Financial support for participation at the ICCE'14 was provided by Virginia Tech.

References

L. Bjerrum. Geotechnical problems involved in foundations of structures in the North Sea. *Geotechnique*, 23(3):319–358, 1973.

T. Butt, P. Russell, and I. Turner. The influence of swash infiltration–exfiltration on beach face sediment transport: onshore or offshore? *Coastal Engineering*, 42(1):35–52, 2001.

E. C. Clukey, F. H. Kulhawy, P. L.-F. Liu, and G. B. Tate. The impact of wave loads and pore-water pressure generation on initiation of sediment transport. *Geo-marine letters*, 5(3):177–183, 1985.

R. W. Dalrymple. Wave-induced liquefaction: a modern example from the Bay of Fundy. *Sedimentology*, 26(6):835–844, 1979.

P. De Wit and C. Kranenburg. The wave-induced liquefaction of cohesive sediment beds. *Estuarine, Coastal and Shelf Science*, 45(2):261–271, 1997.

A. E. Hay, L. Zedel, and N. Stark. Sediment dynamics on a steep, megatidal, mixed sand-gravel-cobble beach. *In print: Earth Surface Dynamics, Special Issue: Frontiers in river, coastal and estuarine morphodynamics*, 2014.

D. P. Horn. Beach groundwater dynamics. *Geomorphology*, 48:121–146, 2002.

D. Jeng. Wave-induced liquefaction potential at the tip of a breakwater: an analytical solution. *Applied Ocean Research*, 18(5):229–241, 1996.

D.-S. Jeng, D. F. Cha, and M. Blumenstein. Neural network model for the prediction of wave-induced liquefaction potential. *Ocean Engineering*, 31(17):2073–2086, 2004.

B. Mutlu Sumer. *Liquefaction around marine structures*. World Scientific, 2014.

B. Mutlu Sumer, F. Hatipoglu, J. Fredsøe, and S. Kaan Sumer. The sequence of sediment behaviour during wave-induced liquefaction. *Sedimentology*, 53(3):611–629, 2006.

M. Nataraja and H. Gill. Ocean wave-induced liquefaction analysis. *Journal of Geotechnical Engineering*, 109(4):573–590, 1983.

P. Nielsen, S. Robert, B. Møller-Christiansen, and P. Oliva. Infiltration effects on sediment mobility under waves. *Coastal Engineering*, 42(2):105–114, 2001.

V. Osinov. Wave-induced liquefaction of a saturated sand layer. *Continuum Mechanics and Thermodynamics*, 12(5):325–339, 2000.

T. Sakai, K. Hatanaka, and H. Mase. Wave-induced effective stress in seabed and its momentary liquefaction. *Journal of waterway, port, coastal, and ocean engineering*, 118(2):202–206, 1992.

S. Sassa and H. Sekiguchi. Wave-induced liquefaction of beds of sand in a centrifuge. *Geotechnique*, 49 (5):621–638, 1999.

S. Sassa and H. Sekiguchi. Analysis of wave-induced liquefaction of sand beds. *Geotechnique*, 51(2): 115–126, 2001.

N. Stark, A. E. Hay, C. Lake, and R. Cheel. The impact of particle shape on friction angle and resulting critical shear stress: An example from a coarse-grained, steep, megatidal beach. *In print: Earth Surface Dynamics, Special Issue: Frontiers in river, coastal and estuarine morphodynamics*, 2014.

N. Stark, A. E. Hay, and L. Zedel. Short-term grain size variability and cobble transport patterns at a steep, megatidal, mixed-sand-gravel beach: Observations from advocate beach, nova scotia. *in prep. for Marine Geology*, in prep.

E. B. Thornton and R. Guza. Transformation of wave height distribution. *Journal of Geophysical Research: Oceans (1978–2012)*, 88(C10):5925–5938, 1983.

I. L. Turner and G. Masselink. Swash infiltration-exfiltration and sediment transport. *Journal of Geophysical Research: Oceans (1978–2012)*, 103(C13):30813–30824, 1998.

I. L. Turner, P. E. Russell, and T. Butt. Measurement of wave-by-wave bed-levels in the swash zone. *Coastal Engineering*, 55(12):1237–1242, 2008.